Indian Journal of Pure & Applied Physics
Vol. 60, January 2022, pp. 72-77

# ZnO Nanoneedle Based Efficient UV-Photodetector

U B Memon[a,b*], A Ibrahim[c], S Roy[d], S P Duttaguptta[b] & S Kale[e]

[a*]Indian Institute of Technology Bombay, Monash Research Academy, Mumbai 400 076,, India

[b]Department of Electrical Engineering, Indian Institute of Technology Bombay, Mumbai 400 076, India.

[c]Department of Condensed Matter Physics and Materials Science, Tata Institute of Fundamental Research, Mumbai 400 001, India

[d]Centre for Research in Nanotechnology and Science, India Institute of Technology Bombay, Mumbai 400 076, India.

[e]Department of Applied Physics, Defence Institute of Advanced Technology, Pune 411 025, India

*Received 14 August 2021; accepted 16 November 2021*

This article reports the fabrication and characterization of nano-structured ITO/ZnO ultraviolet photodetector. A ZnO thin film was deposited by spray pyrolysis technique followed by interdigitated ITO as electrode deposition by RF sputter. Grazing angle x-ray diffraction (GIXRD) study indicates preferential growth along c-axis (002) of thin-film leading nanoneedle formation which was further confirmed by scanning electron microscopy (SEM) imaging. X-ray photoelectron spectroscopy (XPS) analysis of Oxygen 1s (O 1s) was carried out. A peak was observed at 531.8 eV indicating the presence of oxygen vacancy, 530 eV peak relates to the ZnO phase. The bandgap was determined by the Tauc plot; which was found to be 3.22eV. The donor carrier concentration is found to be $8.85 \times 10^{18}$ $cm^{-3}$ based on room temperature Hall measurement. A near ohmic behaviour was observed which can be interpreted by the existence of high carrier concentration in ZnO. This results in a very thin depletion width of the order of 5nm; therefore, charge transport through the junction is dominated by tunnelling of electrons through depletion width.

**Keywords**: ZnO; UV detector; ITO/ZnO ultraviolet photodetector

## 1 Introduction

Ultraviolet (UV) photodetectors have a wide range of applications. Most of them are focused on environmental monitoring, military application, and astronomy[1]. Such applications require very sensitive devices. The mature silicon (Si) photodetector[2-4] technology has enormous limitations; such as visible region detection, low quantum efficiency in the deep UV region, indirect bandgap, which requires a filter to stop low energy photons. Due to inhibition of Si photodetector technology wide bandgap compound semiconductors (such as ZnO, GaN, SiC, ZnSe, *etc.*) have attracted extensive attention due to their intrinsic visible blindness, and direct bandgap. Additionally, these materials are more chemically and thermally stable. Among them, ZnO has become a more promising material for UV detectors due to high excitation binding energy (60 meV), more radiation hardness, low cost, and easy growth process[5,6].

Several different techniques such as chemical vapour deposition (CVD), molecular beam epitaxy (MBE), plasma arc enhanced chemical vapour deposition, pulsed laser deposition (PLD), solgel, reactive evaporation, sputtering, and spray pyrolysis have been successfully implemented for the deposition of ZnO thin films and nanostructures. Each of the above-mentioned techniques has its advantages and limitations. Among them, spray pyrolysis is a simple and cost-effective route to synthesize thin film for large area deposition.

In this work, transparent conducting oxides are considered as a better replacement to the conventional metals as they reduce the shading effect. In this respect, ITO can be used and it has been reported by several times[7-9]. A Schottky nature of ITO contact on ZnO is observed (barrier height 0.3–0.7 eV)[11] as the metalwork function and electron affinity of ITO and ZnO are 4.7 and 4.2 eV respectively. In contrast, ohmic contact of ITO and ZnO has also been reported by Chiou *et al*.[9,10] but not enough explanation was provided. Moreover, the ultra-violet studies of such contact have not been reported yet.

This work explains the ITO/ZnO ohmic contact characteristics based on studies reported by Ibrahim and co-workers. Where ZnO was deposited by spray pyrolysis method. The thin-film material characteristics and UV sensitivity were also investigated.

*Corresponding author: (E-mail: uzb.mem@gmail.com)

## 2 Experimental

The deposition of ZnO in this work was carried out by the spray pyrolysis technique. The schematic diagram of the deposition technique is shown in Fig. 1. An aqueous solution of 0.16 M was prepared by dissolving Zinc Acetate ($Zn(CH_3COO)_2.2H_2O$) in Ethyl Alcohol ($C_2H_5OH$) and further 10% DI water was added. The solution was deposited on quartz substrate where the substrate was kept at an elevated temperature of 683 K for phase formation. The spray nozzle was kept at a distance of 30 cm from the substrate. The solution was sprayed at a rate of 5 ml per minute; deposition was performed at a normal atmosphere. The possible reaction pathway of ZnO formation is given in the equation given below.

$$Zn(CH_3COO)_2.2H_2O \rightarrow Zn^{2+} + 2CH_3COO^- + 2H_2O \quad \ldots (1)$$

$$C_2H_5OH \rightarrow C_2H_5^+ + OH^- \quad \ldots (2)$$

$$Zn^{2+} + 4OH^- \rightarrow Zn(OH)_4^{2-} \quad \ldots (3)$$

$$Zn(OH)_4^{2-} \rightarrow ZnO \downarrow + H_2O + 2OH^-4) \quad \ldots (4)$$

Patterning of ZnO thin film was done by lithography technique followed by RF sputtering of 100 nm ITO. Fig 2 represents the process flow of the fabricated UV photo detector. Material characterization was done to investigate structural, chemical, and optical studies, further electrical characterization was done. GIXRD was done to

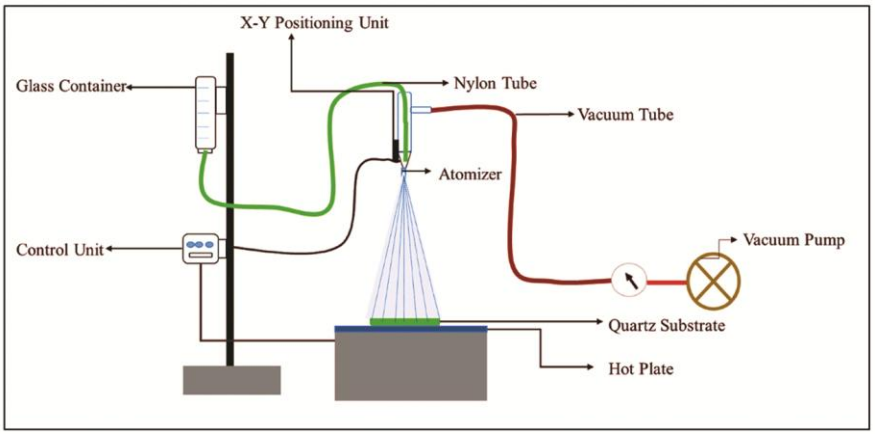


Fig. 1 — Schematic diagram of the deposition technique.

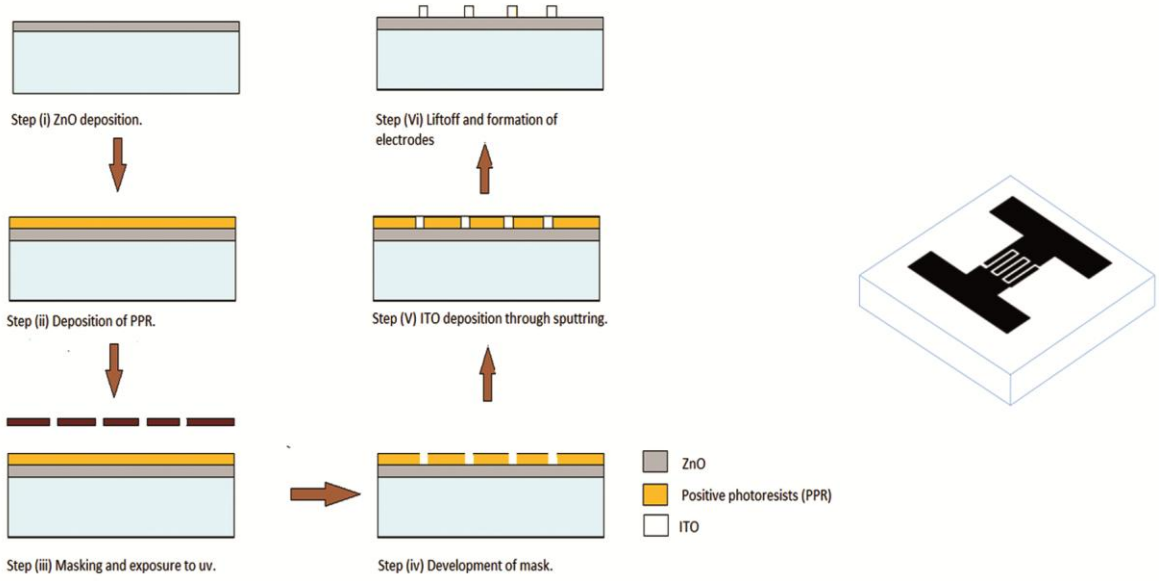


Fig. 2 — Process flow of fabricated UV photodiode.

investigate the crystalline structure of ZnO. Surface morphology was analysed by using Scanning electron microscopy (SEM) (by RAITH II). The chemical state of the fabricated ZnO thin film was determined by using X-ray photoelectron spectroscopy (XPS). The optical properties of the thin film were investigated by using ultra-violet-visible absorption (UV-VIS-NIR) (Parkin Elmer 750). All characterizations were performed at room temperature. The Hall, four-probe, and I–V measurements were performed to investigate the electrical properties. The UV sensitivity was measured by Keithley 2400 under the illumination of a UV lamp of wavelength 285 nm.

## 3 Results and discussions

### 3.1 Crystallinity Studies

The crystallinity studies were investigated using the GIXRD pattern of thin-film shown in Fig 3 was obtained by Cu $K_\alpha$ radiation ($\lambda$=1.5406 Å) at a glancing angle of $0.5^0$. The peak position of (002), (101), (102) (103), and (112) are observed, which corresponds to the wurtzite crystal structure of ZnO (JCPDS S6- 314). The dominating peak along (002) indicates the strong preferred growth along the c-axis. This observation contradicts the JCPDS file (which has dominating peak along the 001 plane) due to the nanostructure growth. The nanostructure is preferably grown along (002) direction to minimize the surface energy, whereas in JCPDS reference the XRD was done of a powder ZnO which has no preferential growth[12,13]. The grain sizes correspond to the peak (002) are estimated by using the Scherrer formula and it was calculated to be 24 nm.

### 3.2 Surface Structure Analysis

SEM imaging was done to determine the surface structure of the fabricated thin film (shown in Fig 4). A regular pattern of nanoneedle of average size 10 to 30 nm can be observed; which is in close agreement with GIXRD results. As observed in XRD analysis the preferential growth along with the c- axis leads to growth along perpendicular to the substrate. Which eventually results in the formation of a needle-like structure. A leaf-like structure was also observed which could be caused by the agglomeration of nanoneedles.

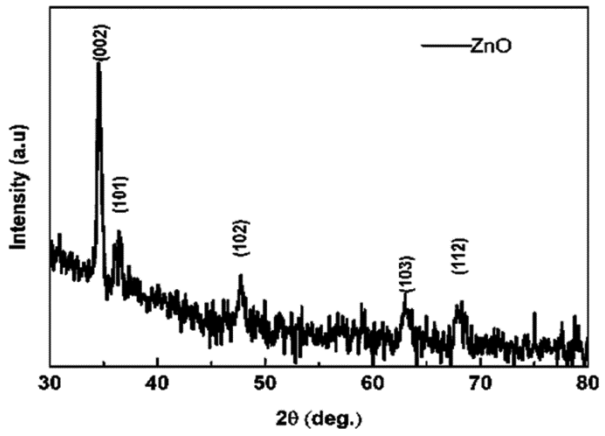


Fig. 3 — GIXRD pattern of ZnO thin film on quartz.

### 3.3 Chemical State Analysis

The XPS survey scan of ZnO thin film is shown in Fig 5. The two peaks at 1022 eV and 1045 eV corresponds to $Zn2p_{3/2}$ and $Zn2p_{1/2}$, respectively. This observation indicates the presence of Zn in the sample is in the chemical state of $Zn^{2+}$ which contributes to the wurtzite structure[14]. The inset shows the $Zn2p_{3/2}$ spectrum; the peak position at 1021.8 eV indicates that pure ZnO was formed.

To further investigate the film, $O1s$ spectral analysis was performed. Two overlapping peaks at

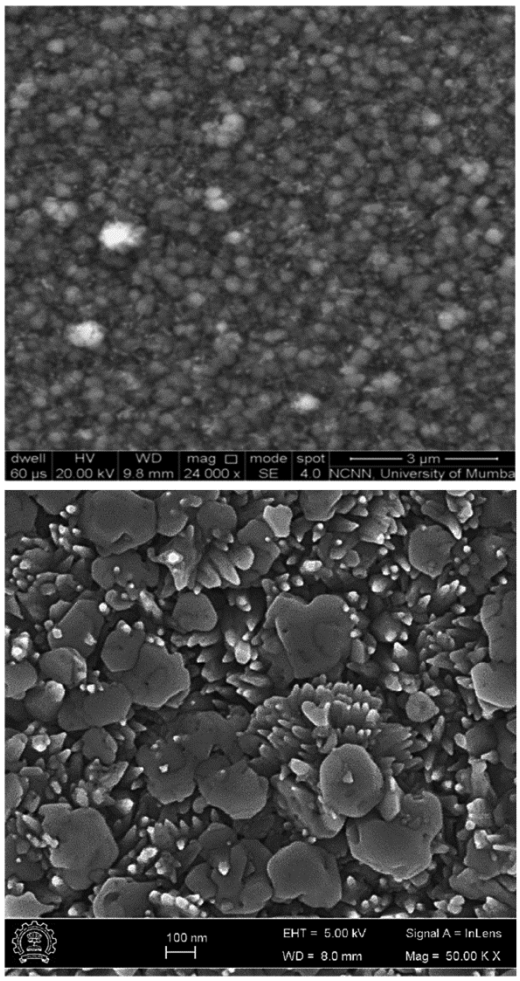


Fig. 4 — SEM image of ZnO film deposited by spray pyrolysis.

530 and 531.8eV were observed (Fig 6). The peak at 530.0 was attributed to the presence of $O^{2-}$ ion in the $Zn^{2+}$ array of the wurtzite structure. Whereas the higher energy peak position at 531.8 eV is associated with the presence of oxygen deficiency in the film[14,15]. It is noticeable from Fig 6 that the peak intensity at 531.8 eV is higher than that at 530 eV. This observation reveals that the presence of oxygen vacancy ($V_0$) is higher in comparison to $O^{2-}$ in the $Zn^{2+}$ array.

### 3.4 UV-VIS-NIR

UV-VIS-NIR spectroscopy was performed to calculate the bandgap of ZnO. The bandgap was determined by the Tauc plot (Fig 7) and it was found to be 3.22 eV. The observed bandgap is much lower than bulk ZnO film (3.37 eV). The redshift in bandgap is due to the presence of oxygen vacancies in ZnO. Therefore, this observation correlates with the results obtained by XPS. It was reported by Wang *et al.*[16] that due to the presence of oxygen vacancies the impurity states become delocalize and overlaps with the valence band edge. Consequently, the apparent valence band shifts upwards, and accordingly bandgap narrowing occurs. According to many reports, the presence of oxygen vacancy does not contribute to n-type carrier concentration in ZnO, as it creates a deep donor states level close to the valence band. In our work, we have observed that the increase of oxygen vacancy leads to an increase in n-type carrier concentration which was confirmed by Hall measurement. Such discrepancy was explained by Kim *et al*[17]. Where they demonstrated the phenomenon of the formation of $V_0$–$Z_{ni}$ (Zn interstitial) bond. As a result, such a complex might generate electrons which contribute to the conduction of electrons. Hence, an increase in $V_0$ contributes to more electron generation.

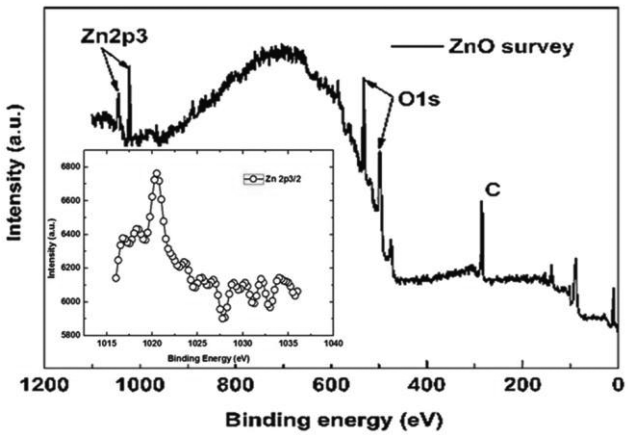


Fig. 5 — Survey scan of ZnO film.

### 3.5 Electrical Characterization

Electrical characterization such as Hall and Four probe measurement was performed to validate the observation of XPS and UV-VIS-NIR of ZnO. The carrier concentration and resistivity were found to be $8.85\times10^{18}$ $cm^{-3}$ and 0.09 Ω–cm respectively. The presence of high oxygen vacancy as proposed by Kim *et al*[17] attributes to high carrier concentration. The current-voltage measurement (I–V) of ITO/ZnO is shown in Fig 8.

Near ohmic behaviour was observed. This can be realized by tunnelling of electrons through the depletion width of ITO/ZnO. As carrier concentration is high, the Fermi energy level goes up to the conduction band ($N_C = 4\times10^{18}$ $cm^{-3}$)[18]. Hence, under

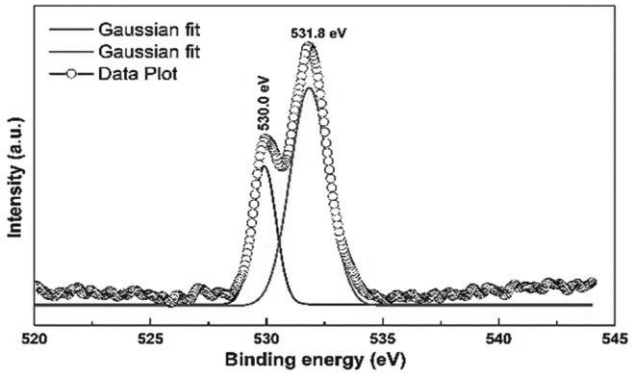


Fig. 6 — O 1s XPS spectroscopic spectra of the ZnO samples.

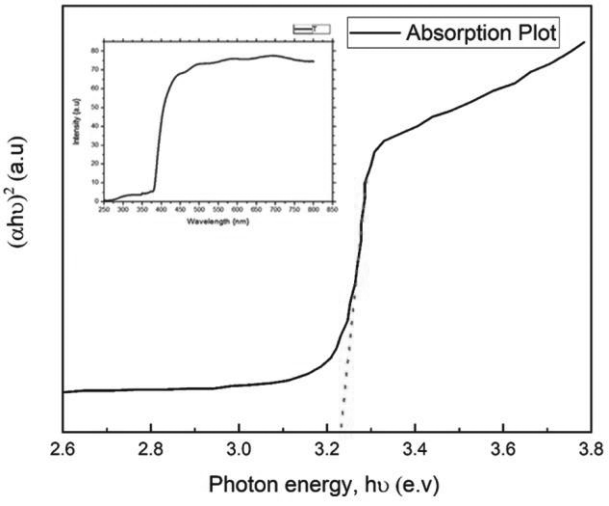


Fig. 7 — UV-VIS-NIR spectrum for bandgap calculation; inset shows the transmission spectrum of ZnO.

bias conditions electrons do not conduct by thermionic emission, rather it tunnels through the barrier, as a result, the tunnelling current dominates[19]. To find the possibility of electron tunnelling, the depletion width was calculated; which was found to be 5 nm. The band diagram of ITO/ZnO contact (not scaled) under bias condition is shown in Fig 9.

### 3.6 UV sensing

The dark and UV illuminated I–V characteristics of thin-film are demonstrated in Fig 10. The illumination was done under a 285 nm irradiation source. The current versus applied voltage was plotted in the log as well as the linear scale. A significant (10 times at ±2 V) change of device current can be observed on the illumination of UV light.

The response time of the device was investigated as shown in Fig 11. The rise and decay time of the device was found to be 7 and 13 Sec, which is comparable to the previously reported values[20,21]. The decay time is expected to be fast as the electron transportation is dominated by tunnelling through the barrier, but a large decay time has been observed which can be explained as follows. The photogenerated hole get captured to $V_0$ and get transformed to $V_0^+$ or $V_0^{2+}$. The defects and trap play an important role and decide the overall efficacy of the performance. Charge carriers (electron and holes) are lost at the interface due to high interface defect density. Moreover, the shunt resistance ($R_{SH}$) at ZnO/ITO interface results in the instability and performance degradation of the device[22]. These defect states start capturing the free electron from the sample as the irradiation stops. This process is responsible for the persistence of optical current. Figs 12(a) represent the sensing setup and 12(b) represent the UV response of the photodetector at biasing voltage of 0.2 volt. Table 1 summarize the material properties for an efficient UV photodetector.

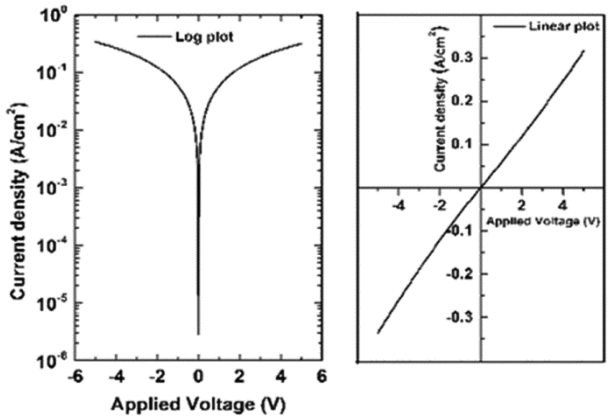


Fig. 8 — I–V plot of ITO/ZnO contact.

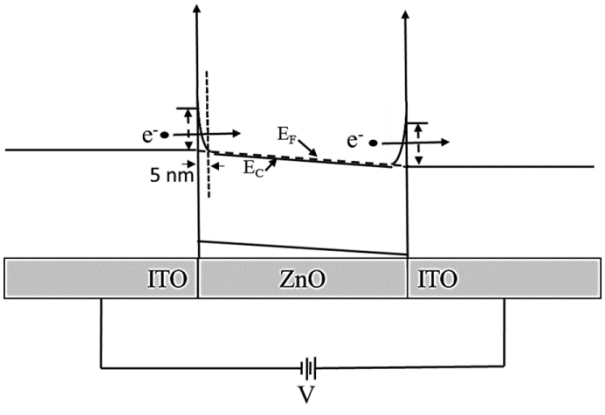


Fig. 9 — Band diagram of ITO/ZnO contact under bias condition non illumination of UV light.

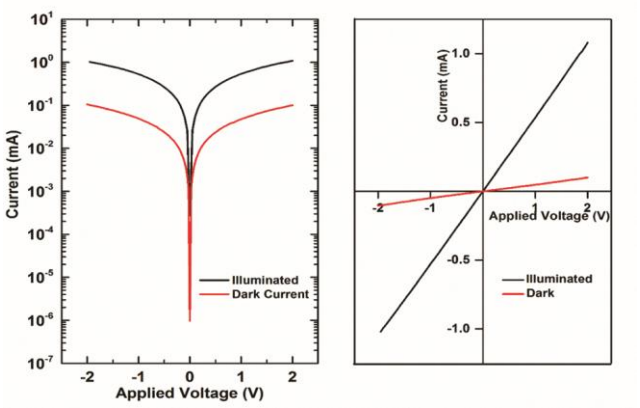


Fig. 10 — Current-voltage characteristics of ZnO under UV and in dark conditions.

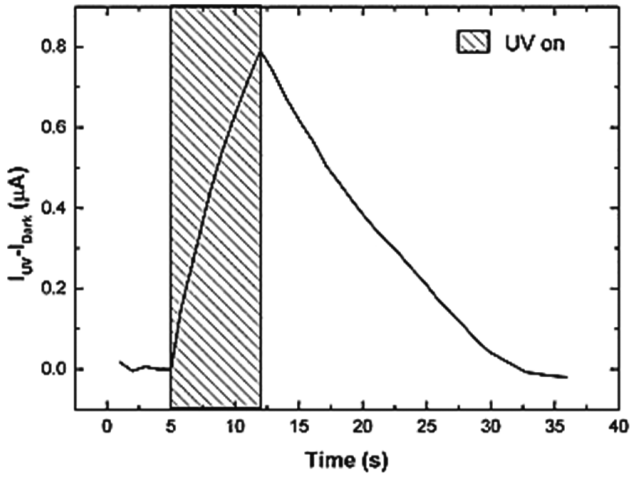


Fig. 11 — Photo response of the device under a bias condition 0.l.

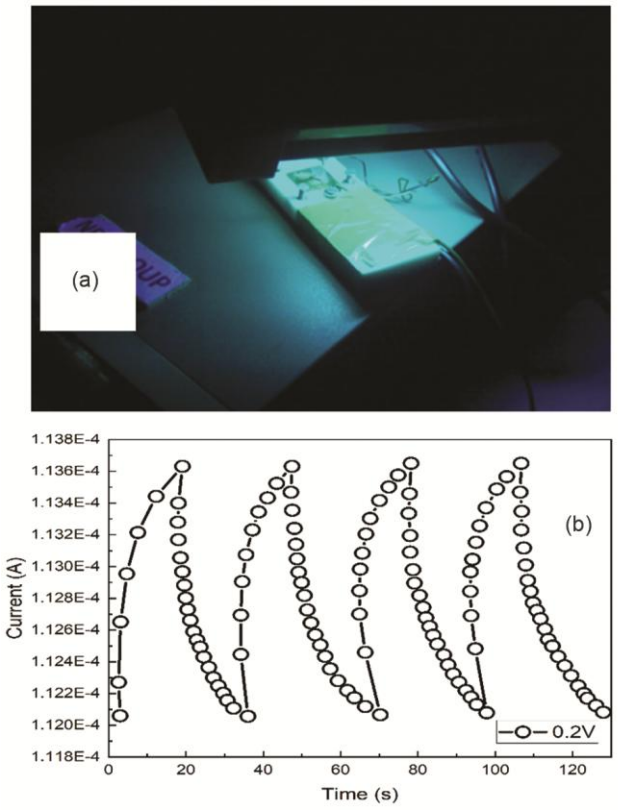


Fig. 12 — (a) represents UV photodetector setup (b) represents UV sensing at 0.2 V.

Table 1 — ZnO material properties for an efficient UV photodetector

| | ZnO material properties | |
|---|---|---|
| 1 | Average particle size | 10 to 30 nm |
| 2 | Carrier concentration | $8.85\times10^{18}$ $cm^{-3}$ |
| 3 | Resistivity | 0.09 Ω–cm |
| 4 | Bandgap | 3.22 eV |
| 5 | Grain size | 24 nm |

## 4 Conclusion

In summary, ZnO nanoneedle deposition was performed by the spray pyrolysis technique. Various thin film characterizations were done and it was observed that a significant amount of oxygen vacancy was present in the film. These oxygen vacancies contribute to the high n-type carrier concentration. Further interdigitated ITO electrode was deposited on the film. The ITO/ZnO contact was found to be ohmic rather than Schottky, which is due to dominating electron tunnelling. The device was further characterized as a UV sensor. Promising behaviour was observed under UV illumination. The rise and decay response time under illumination was observed to be better than previously reported values.

## Acknowledgment

This work was supported by the IIT-Bombay Nanofabrication facility, Mumbai India 400076. We are thankful to Mr. Sandip Dhobale, Pune University for helping us in thin film deposition. We would also like to acknowledge DIAT Pune for the fabrication facility.

## Reference

1 Liu K, Sakurai M & Aono M, *Sensors*, 10 (2010) 8604.
2 Shi L & Nihtianov S, *IEEE Sens J*, 12 (2012) 2453.
3 Roy S, Midya K, Duttagupta S P & Ramakrishnan D, *J Appl Phys*, 16 (2014) 1.
4 Casalino M, Coppola G, Iodice M, Rendina I & Sirleto L, *Sensors*, 10 (2010) 10571.
5 Bai S, Wu W, Qin Y, Cui N, Bayerl D J & Wang X, *Adv Funct Mater*, 21 (2011) 4464.
6 Suhail A M, Hassan E K, Ahmed S S & Alnoori M K M, *Power*, 8 (2010) 268.
7 Lee H Y, Su C T, Wu B K, Lin Y J & Chern M Y, *Jpn J Appl Phys*, 50 (2011) 9.
8 Yoon J G, Cho S W, Lee E & Chung J S, *Appl Phys Lett*, 95 (2009) 1.
9 Chiou Y Z & Lin K W, *J Electrochem Soc*, 153 (2006) 141.
10 Ahmad G, Mandal S, Barua A K, Bhattacharyya T K & Roy J N, *IEEE J Photovoltaics*, 8 (2018) 8.
11 Lee H Y, Wu B K & Chern M Y, *Appl Phys Express*, 6 (2013) 4.
12 Young S J, Ji L W, Cheng S J, Chen Y P, Peng S M, *Semicond Sci Technol*, 23 (2008) 085016.
13 Hadjeris L, Herissi L, Assouar M B, Easwarakhanthan T, Bougdira J, Attaf N & Aida M S, *Semicond Sci Technol*, 24 (2009) 035006.
14 Ansari S A, Khan M M, Kalathil S, Nisar A, Lee J & Cho M H, *Nanoscale*, 5 (2013) 9238.
15 Park S M, Ikegami T & Ebihara T, *Thin Solid Films*, 513 (2006) 90.
16 Wang J, Wang Z, Huang B, Ma Y, Liu Y, Qin X, Zhang X & Dai Y, *ACS Appl Mater Interfaces*, 4 (2012) 4024.
17 Kim D H, Lee G W & Kim Y C, *Solid State Commun*, 152 (2012) 1711.
18 Abdolahzadeh Z & Rozati S M, *Phys B Condens Matter*, 407 (1981) 4512.
19 *Physics of Semiconductor Devices* (2nd Edition), by Sze S M A, wiley Interscience Publication.
20 Hong S, Yeo J, Manorotkul W, Kim G, Kwon J, An K & Ko S H, *J Nanomater*, 2013 (2013).
21 Panda S K & Jacob C, *Solid State Electron*, 73 (2012) 44.
22 Gufran A, Das G & Roy J N, *J Mater Sci: Mater Electron*, 30 (2019) 12406.